1st International Conference of the
International Journal of Structural Integrity
June 25-28, 2012, Porto, Portugal

Mixed-Mode Fracture Toughness Determination

USING NON-CONVENTIONAL TECHNIQUES

Filipe J.P.Chaves

IDMEC- Pólo FEUP

L.F.M. da Silva

M.F.S.F. de Moura

DEMec - FEUP

D. Dillard

ESM – Virginia Tech

motivation

fracture modes

conventional tests [mode I]

conventional tests [mode II]

conventional tests [mixed-mode I + II]

non-conventional tests [mixed-mode I + II]

conclusions

acknowledgments

outline

Boeing 737

Aloha Flight 243

Photos from NTSB

Bonded joints in service are usually subjected to mixed-mode conditions due to geometric and loading complexities.

Consequently, the fracture characterization of bonded joints under mixed-mode loading is a fundamental task.

There are some conventional tests proposed in the literature concerning this subject, as is the case of the asymmetric double cantilever beam (ADCB), the single leg bending (SLB) and the cracked lap shear (CLS).

Nevertheless, these tests are limited in which concerns the variation of the mode-mixity, which means that different tests are necessary to cover the fracture envelope in the G_I-G_{II} space.

This work consists on the analysis of the different mixed mode tests already in use, allowing to design an optimized test protocol to obtain the fracture envelope for an adhesive, using a Double Cantilever Beam (DCB) specimen.

motivation

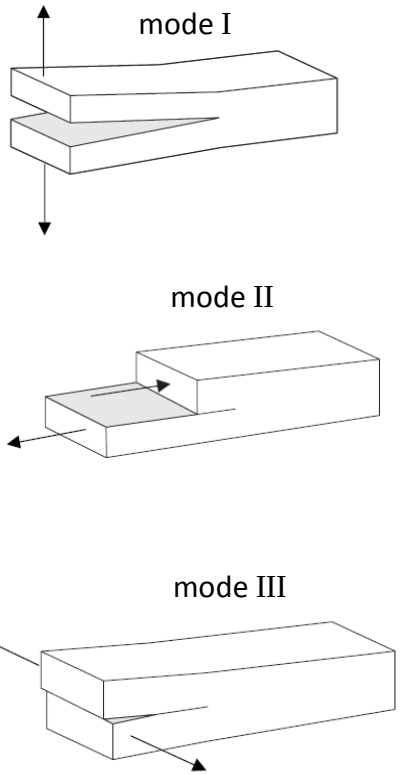

Figure 1. Fracture modes.

Mode I – opening mode (a tensile stress normal to the plane of the crack);

Mode II – Sliding mode (a shear stress acting parallel to the plane of the crack and perpendicular to the crack front);

Mode III – tearing mode (a shear stress acting parallel to the plane of the crack and parallel to the crack front)

fracture modes

Mode I release rate energy G_I is well known and well characterized.

DCB – Double Cantilever Beam

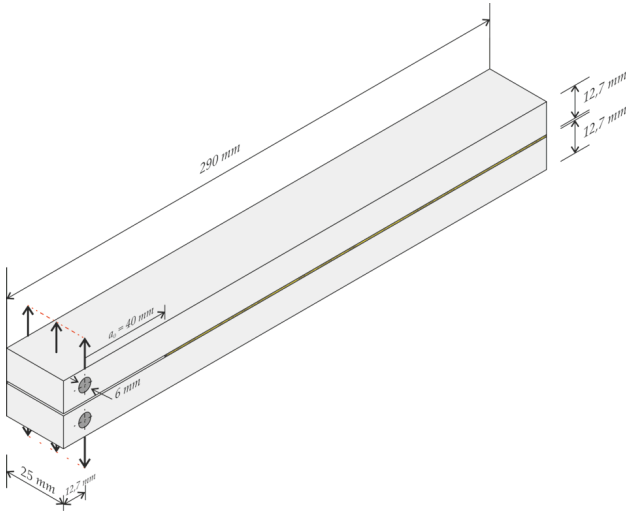

Figure2. DCB specimen and test.

&

ASTM D 3433 - 99

TDCB – Tapered Double Cantilever Beam

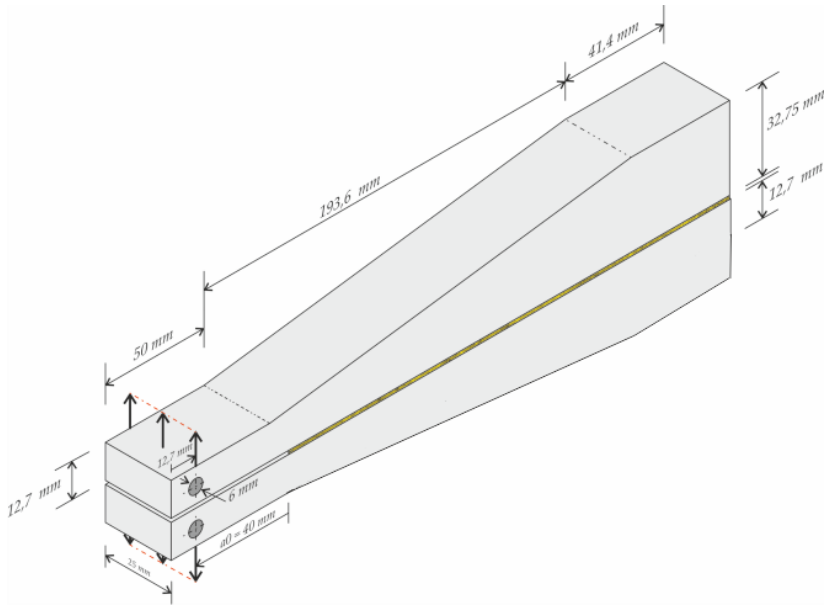

Figure 3. TDCB specimen and test.

conventional tests [mode I]

ENF – End Notch Flexure

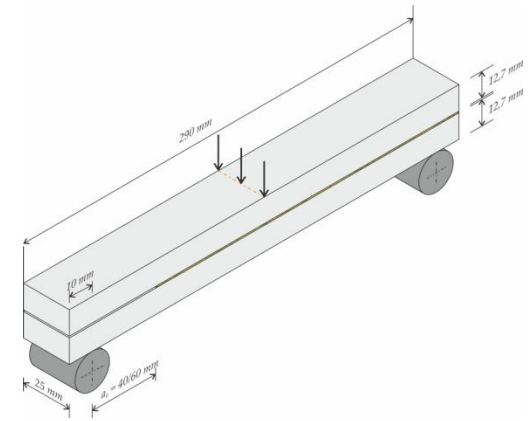

Figure 4. ENF specimen and test.

4ENF - 4 Points End Notch

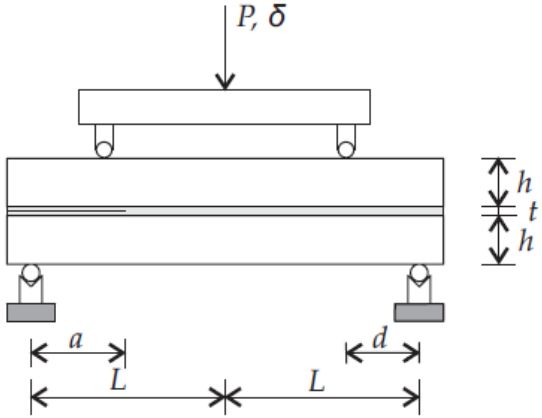

Figure 5. 4 ENF scheme

ELS – End Load Split

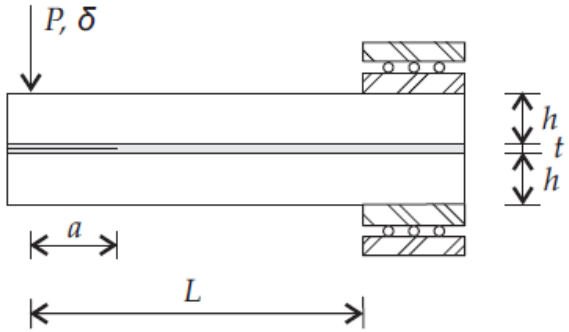

Figure 6. ELS scheme

conventional tests [mode II]

Mixed-Mode I + II release rates energies $G_T = G_{IC} + G_{IIC}$.

CLS - Crack Lap Shear

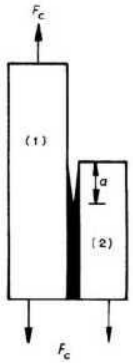

EDT - Edge Delamination Tension

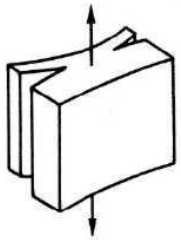

Arcan

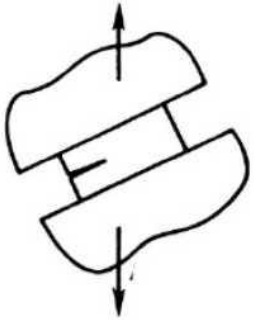

MMF - Mixed Mode Flexure

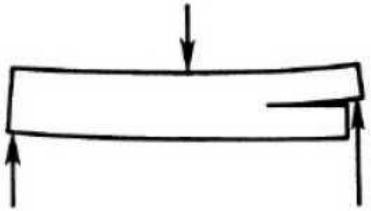

Mixed Mode Bending [MMB] **ASTM D6671**

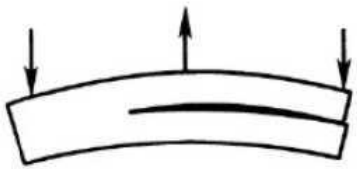

Asymmetrical Double Cantilever Beam [ADCB]

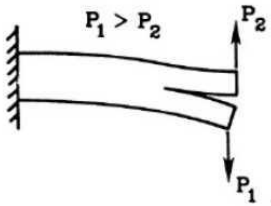

Asymmetrical Tapered Double Cantilever Beam [ATDCB]

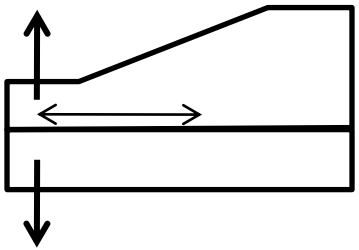

SLB – Single Leg Bending

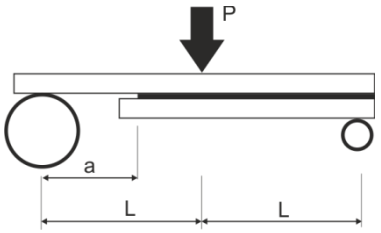

Figure 7. Conventional test schemes for mixed-mode I + II.

conventional tests [mixed-mode I+II]

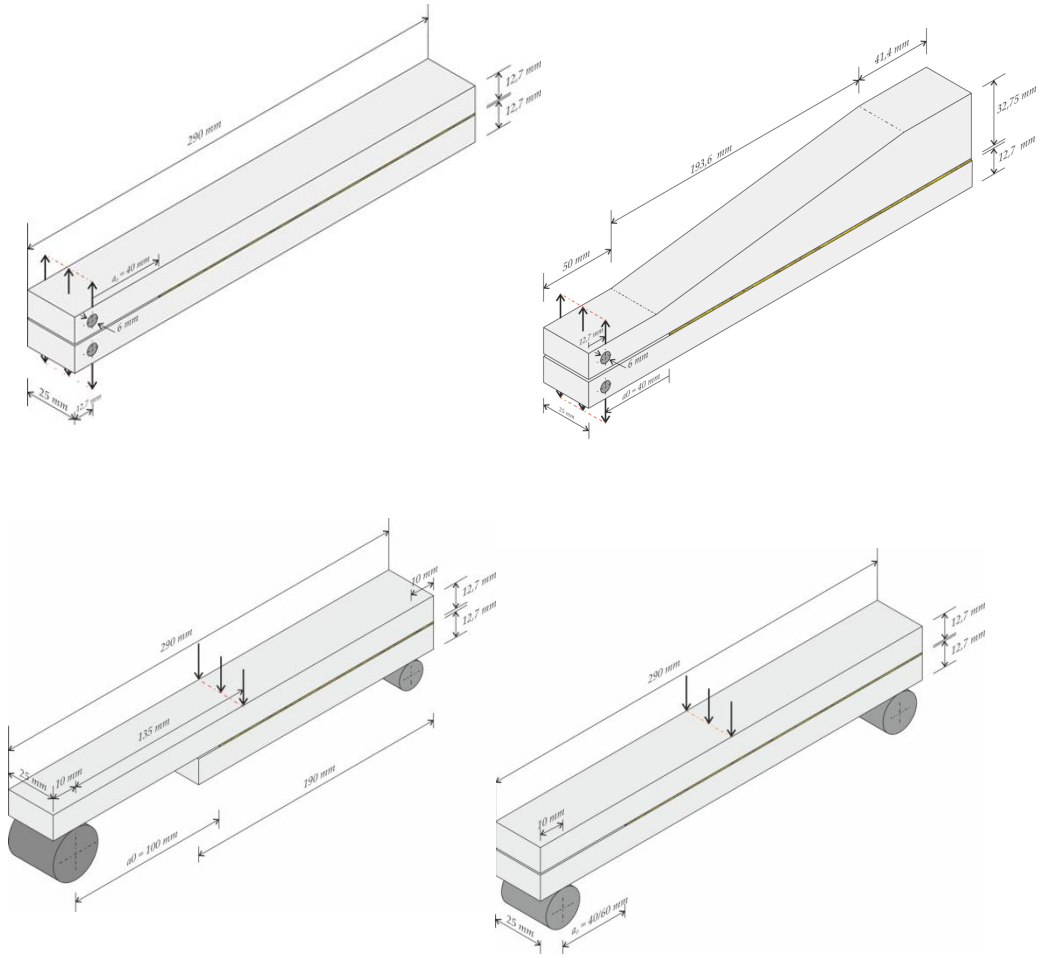

Figure 8. DCB, ATDCB, SLB and ENF specimen geometries.

Bondline thickness = 0.2 mm

Table1. Adhesive shear properties using the thick adherend shear test method ISO 11003-2

	Araldite 2015
Shear modulus G (MPa)	487 ± 77
Shear yield strength τ_{ya} (MPa)	17.9 ± 1.80
Shear strength τ_r (MPa)	17.9 ± 1.80
Shear failure strain γ_f (%)	43.9 ± 3.40

Table2. Steel adherend properties

Steel	DIN 40CrMnNiMo7.
Young modulus, E [Gpa]	205
Yield strength, σ_y [MPa]	~ 900
Shear strength, σ_y [MPa]	~ 1000
Strain, ε_f [%]	~ 15

conventional tests

Table 3. Fracture toughness obtained with the conventional testing methods (average and standard deviation).

Test type	G_{Ic} (N/mm)	G_{IIc} (N/mm)
DCB+	0.44 ± 0.05	–
ENF	–	2.1 ± 0.21
SLB*	0.34 ± 0.06	0.32 ± 0.06
ADCB*	0.41 ± 0.04	0.004 ± 0.0005
ATDCB*	0.32 ± 0.04	0.07 ± 0.006

\+ Value corresponding to CBBM

* For these tests, the values indicated correspond to G_I and G_{II} and not G_{Ic} and G_{IIc}.

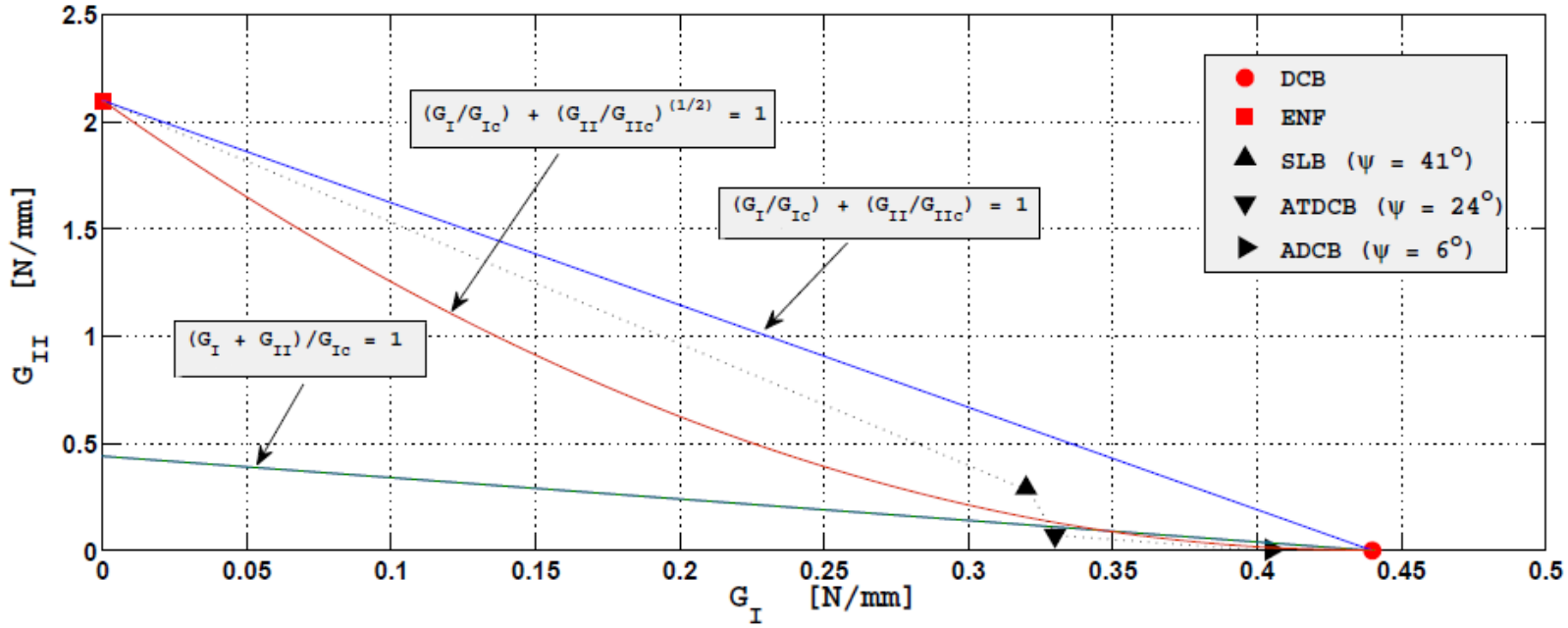

Figure 9. Fracture envelope for conventional tests.

conventional tests [envelope]

Designation: D 6671/D 6671M

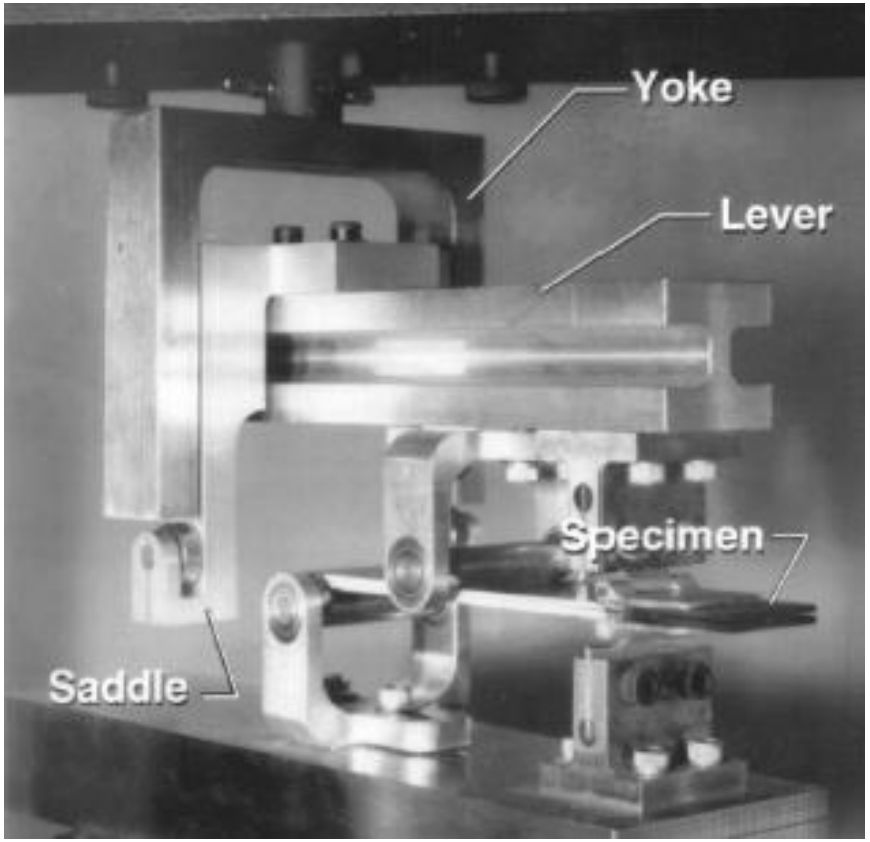

Figure 10. Modified Mixed Mode Bending by Reeder.

Compliance Based Beam Method applied to MMB

J.M.Q. Oliveira et al. / Composites Science and Technology **67** (2007) 1764–1771

$$G_I = \frac{12a_{eq,I}^2 P_I^2}{B^2 h^3 E_{fI}} + \frac{6P_I^2}{5B^2 hG} \quad (1)$$

$$G_{II} = \frac{9a_{eq,II}^2 P_{II}^2}{16B^2 h^3 E_{fII}} \quad (2)$$

An equivalent crack length ($a_{eq,I}$ and $a_{eq,II}$) can be obtained from the previous equation as a function of the measured current compliance $a_{eq,I} = f(C_I)$ and $a_{eq,II} = f(C_{II})$

- conventional tests [mixed-mode I+II]

The specimen was modelled with 11598 plane strain 8-node quadrilateral elements and 257 6-node interface elements with null thickness placed at the mid-plane of the bonded specimen.

ABAQUS®

Table 4. Elastic and cohesive properties.

Elastic properties (Steel)		Cohesive properties (Adhesive)			
E (GPa)	G (MPa)	$s_{u,I}$ (MPa)	$s_{u,II}$ (MPa)	G_{Ic} (N/mm)	**G_{IIc} (N/mm)**
210	**80.77**	**23**	**23**	**0.6**	**1.2**

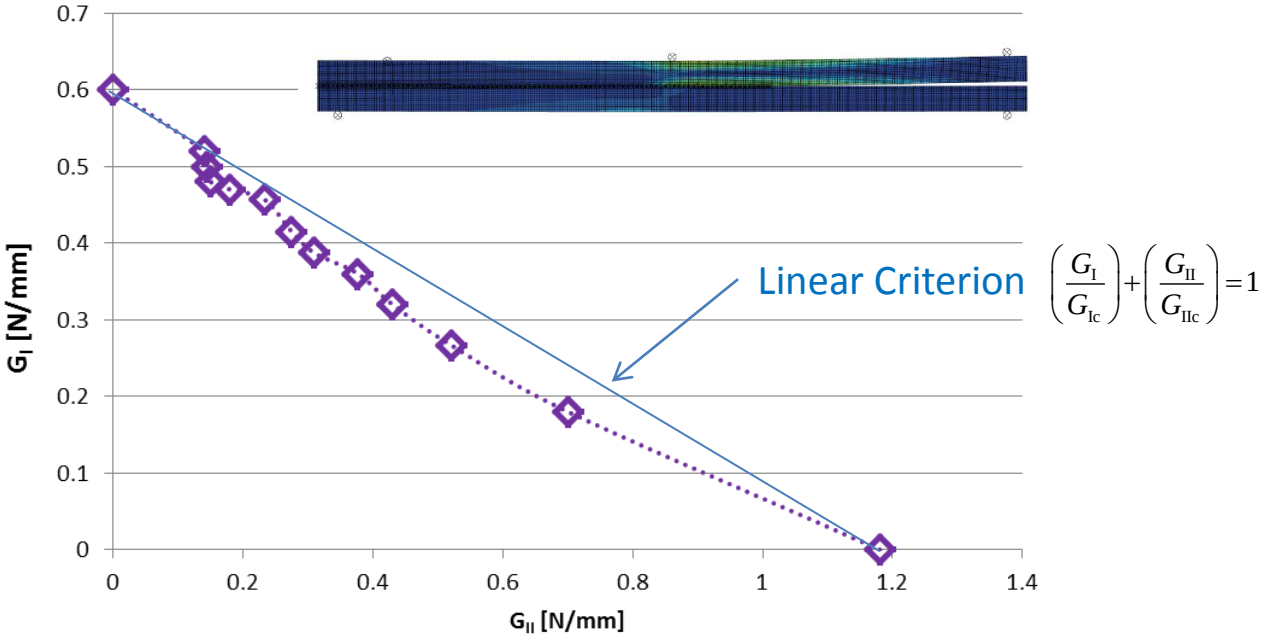

Figure 11. Numerical Fracture Envelope for MMB.

conventional tests [mixed-mode I+II]

The Dual Actuator Load Frame (DAL) test is based on a DCB specimen loaded asymmetrically by means of two independent hydraulic actuators

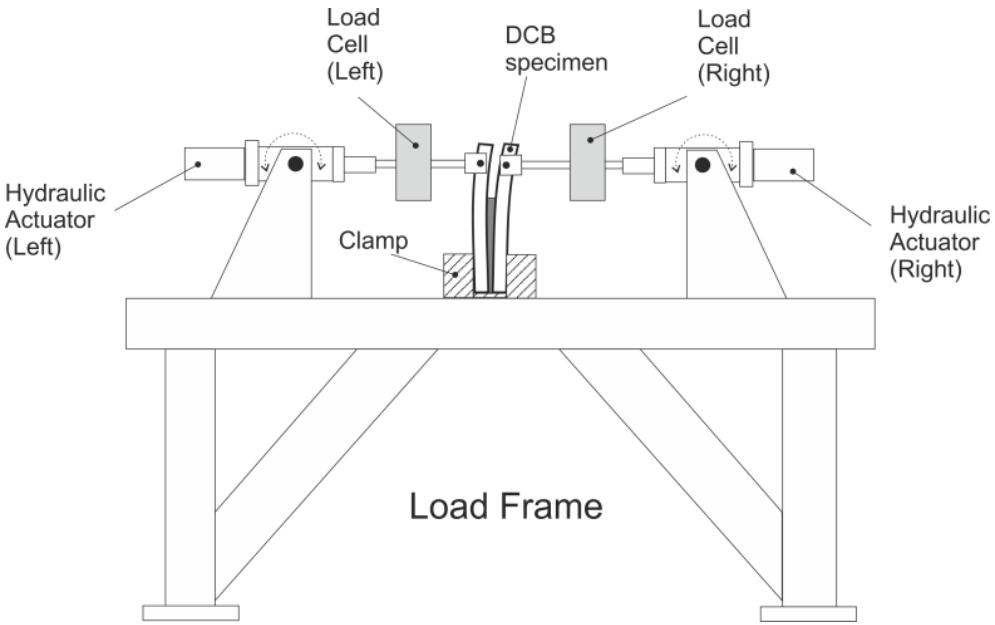

Figure 13. DAL frame

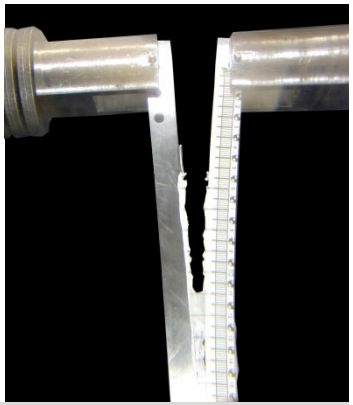

Figure 12. DAL loading a DCB specimen.

Different combinations of applied displacement rates provide different levels of mode ratios, thus allowing an easy definition of the fracture envelope in the G_I versus G_{II} space.

non-conventional tests [mixed-mode I+II]

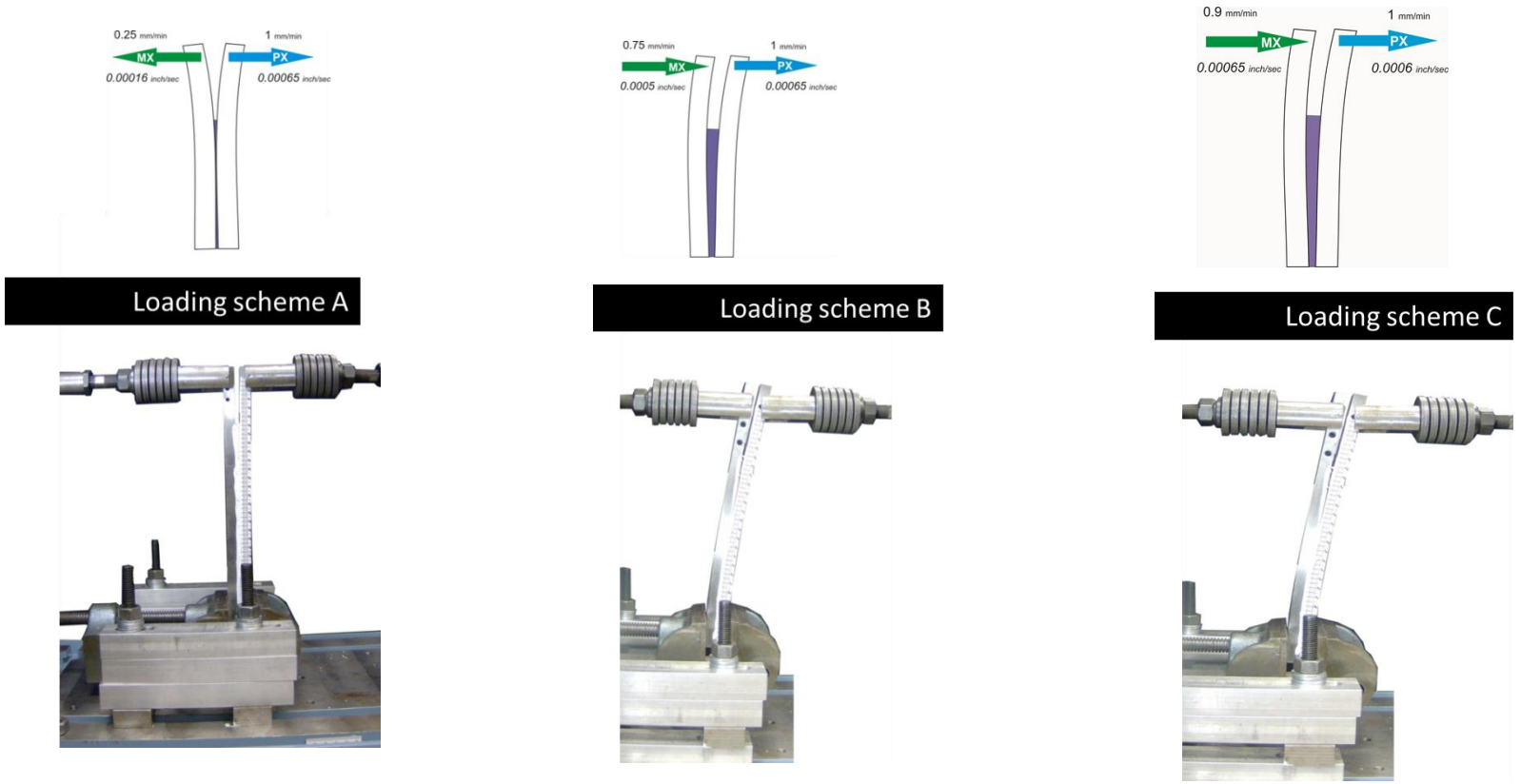

Figure 14. Loading schemes.

Classical data reduction schemes based on compliance calibration and beam theories require crack length monitoring during its growth, which in addition to FPZ ahead of the crack tip can be considered important limitations.

- non-conventional tests [mixed-mode I+II]

Using Timoshenko beam theory, the strain energy of the specimen due to bending and including shear effects is:

$$U = \int_0^a \frac{M_R^2}{2EI_R}dx + \int_0^a \frac{M_L^2}{2EI_L}dx + \int_a^L \frac{M_T^2}{2EI}dx + \int_0^a \int_{-h/2}^{h/2} \frac{\tau_R^2}{2G} B\,dydx + \int_0^a \int_{-h/2}^{h/2} \frac{\tau_L^2}{2G} B\,dydx + \int_a^L \int_{-h}^{h} \frac{\tau_T^2}{2G} B\,dydx \quad (3)$$

M is the bending moment

subscripts R and L stand for right and left adherends

T refers to the total bonded beam (of thickness 2*h*)

E is the longitudinal modulus

G is the shear modulus

B is the specimen and bond width

I is the second moment of area of the indicated section

For adherends with same thickness, considered in this analysis, $I = 8I_R = 8I_L$

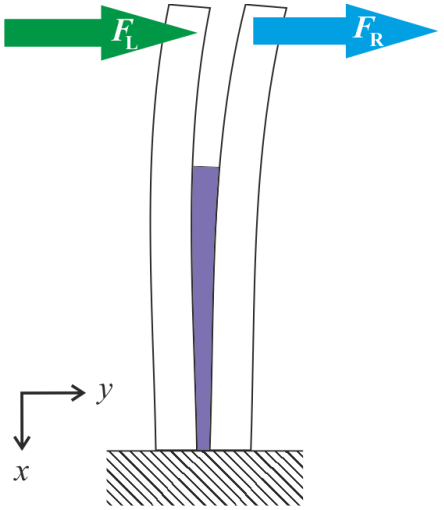

Figure 15. Schematic representation of loading in the DAL test.

non-conventional tests [mixed-mode I+II]

The shear stresses induced by bending are given by:

$$\tau = \frac{3}{2}\frac{V}{Bh}\left(1-\frac{y^2}{c^2}\right) \qquad (4)$$

c - beam half-thickness

V - transverse load ⟶ on each arm for $0 \le x \le a$, and on total bonded beam for $a \le x \le L$

From Castigliano's theorem $\delta = \partial U / \partial P$

- P is the applied load
- δ is the resulting displacement at the same point

the displacements of the specimen arms can be written as

$$\delta_L = \frac{\left(7a^3+L^3\right)F_L}{2Bh^3E} + \frac{(L^3-a^3)F_R}{2Bh^3E} + \frac{3L\left[(F_L+F_R)+a(F_L-F_R)\right]}{5BhG}$$

$$\delta_R = \frac{\left(7a^3+L^3\right)F_R}{2Bh^3E} + \frac{(L^3-a^3)F_L}{2Bh^3E} + \frac{3L\left[(F_L+F_R)+a(F_R-F_L)\right]}{5BhG} \qquad (5)$$

non-conventional tests [mixed-mode I+II]

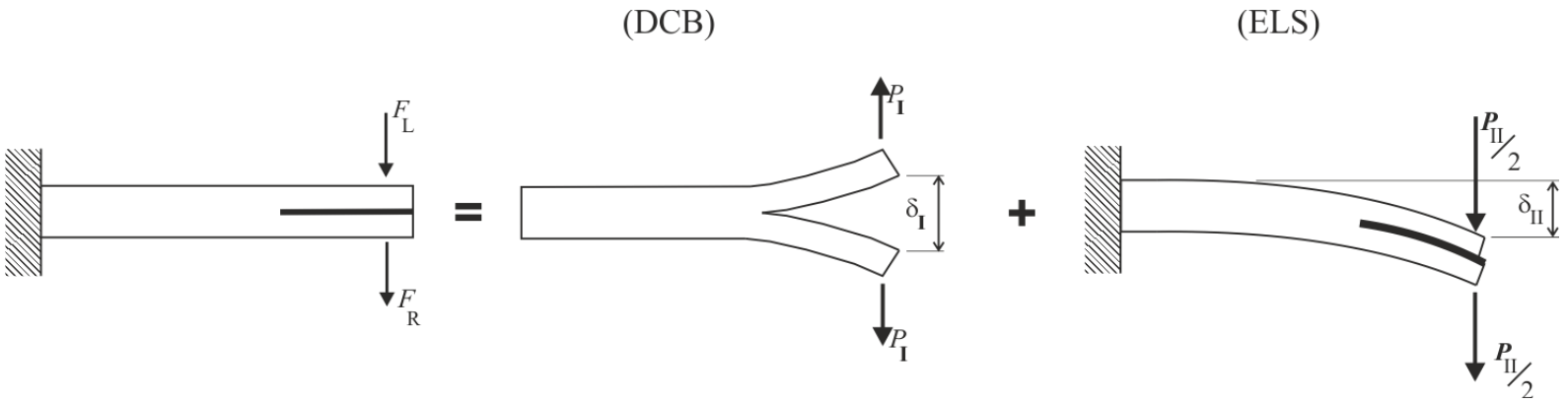

Figure 16. Schematic representation of loading in the DAL test.

pure mode loading

$$P_I = \frac{F_R - F_L}{2} \qquad P_{II} = F_R + F_L \tag{6}$$

pure mode displacements

$$\delta_I = \delta_R - \delta_L \qquad \delta_{II} = \frac{\delta_R + \delta_L}{2} \tag{7}$$

- non-conventional tests [mixed-mode I+II]

Combining equations (5-7), the pure mode compliances become

(8) $$C_{\mathrm{I}} = \frac{\delta_{\mathrm{I}}}{P_I} = \frac{8a^3}{Bh^3E} + \frac{12a}{5BhG}$$ and $$C_{\mathrm{II}} = \frac{\delta_{\mathrm{II}}}{P_{\mathrm{II}}} = \frac{3a^3 + L^3}{2Bh^3E} + \frac{3L}{5BhG}$$ (9)

However, stress concentrations, root rotation effects, the presence of the adhesive, load frame flexibility, and the existence of a non-negligible fracture process zone ahead of crack tip during propagation are not included in these equations

To overcome these drawbacks, equivalent crack lengths can be calculated from the current compliances C_{I} and C_{II} (eq. 6 and 7)

$$\alpha a_{\mathrm{eI}}^3 + \beta a_{\mathrm{eI}} + \gamma = 0$$

$$a_{\mathrm{eI}} = \frac{1}{6\alpha} A - \frac{2\beta}{A} \quad (10)$$

$$a_{\mathrm{eII}} = \left[\left(C_{\mathrm{II}} - \frac{3L}{5BhG} \right) \frac{2Bh^3E}{3} - \frac{L^3}{3} \right]^{1/3} \quad (11)$$

$$\alpha = \frac{8}{Bh^3E}; \quad \beta = \frac{12}{5BhG}; \quad \gamma = -C_{\mathrm{I}}$$

$$A = \left(\left(-108\gamma + 12\sqrt{3\left(\frac{4\beta^3 + 27\gamma^2\alpha}{\alpha} \right)} \right) \alpha^2 \right)^{\frac{1}{3}}$$

- non-conventional tests [mixed-mode I+II]

The strain energy release rate components can be determined using the Irwin-Kies equation:

$$G = \frac{P^2}{2B}\frac{dC}{da} \quad (12)$$

combined with equation 6 →

$$C_{\mathrm{I}} = \frac{\delta_{\mathrm{I}}}{P_I} = \frac{8a^3}{Bh^3E} + \frac{12a}{5BhG}$$

$$G_{\mathrm{I}} = \frac{6P_{\mathrm{I}}^2}{B^2h}\left(\frac{2a_{\mathrm{eI}}^2}{h^2E} + \frac{1}{5G}\right) \quad (13)$$

combined with equation 7 →

$$C_{\mathrm{II}} = \frac{\delta_{\mathrm{II}}}{P_{\mathrm{II}}} = \frac{3a^3 + L^3}{2Bh^3E} + \frac{3L}{5BhG}$$

$$G_{\mathrm{II}} = \frac{9P_{\mathrm{II}}^2 a_{\mathrm{eII}}^2}{4B^2h^3E} \quad (14)$$

- The method only requires the data given in the load-displacement (P-δ) curves of the two specimen arms registered during the experimental test.
- Accounts for the Fracture Process Zone (FPZ) effects, since it is based on current specimen compliance which is influenced by the presence of the FPZ.

non-conventional tests [mixed-mode I+II]

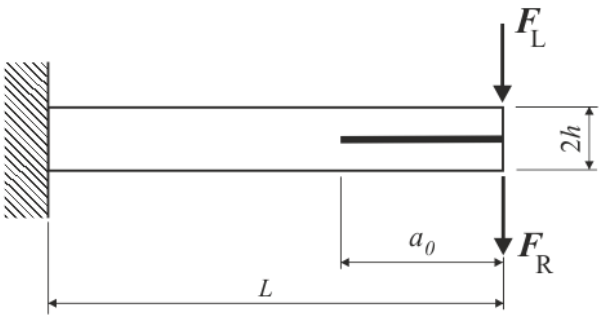

Figure 16. Specimen geometry used in the simulations of the DAL test

Numerical analysis including a cohesive damage model was carried out to verify the performance of the test and the adequacy of the proposed data reduction scheme.

Table 4. Elastic and cohesive properties.

Elastic properties (Steel)		**Cohesive properties (Adhesive)**			
E (GPa)	G (MPa)	$s_{u,I}$ (MPa)	$s_{u,II}$ (MPa)	G_{Ic} (N/mm)	**G_{IIc} (N/mm)**
210	**80.77**	**23**	**23**	**0.6**	**1.2**

The specimen was modelled with 7680 plane strain 8-node quadrilateral elements and 480 6-node interface elements with null thickness placed at the mid-plane of the bonded specimen.

non-conventional tests [mixed-mode I+II]

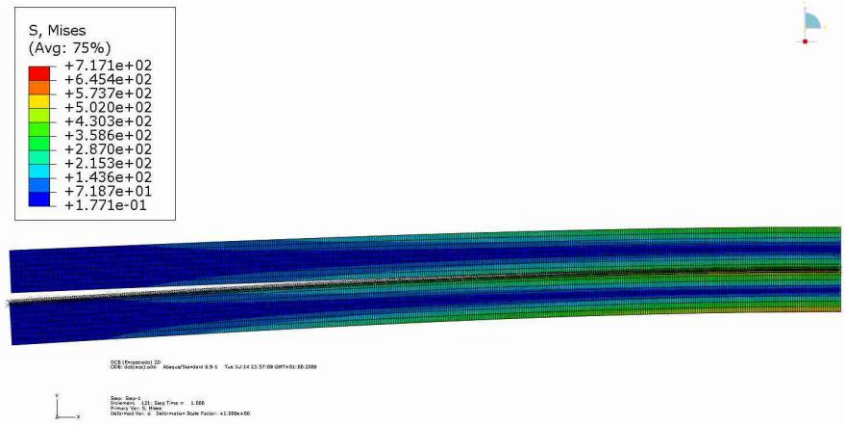

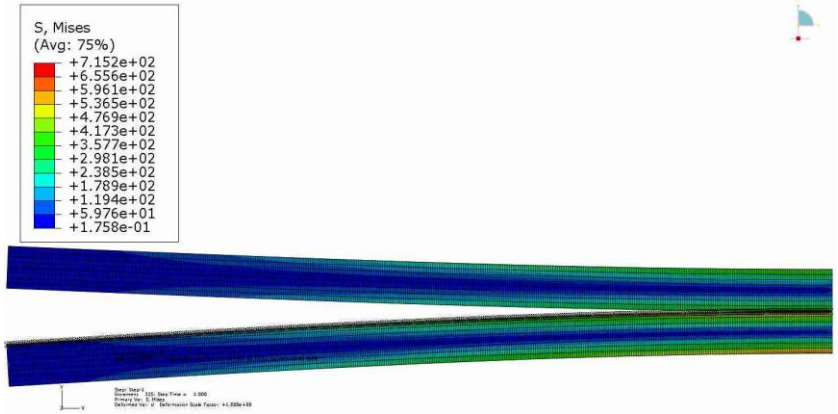

Figure 17. ABAQUS simulation mixed-mode (left) mode I (right)

a

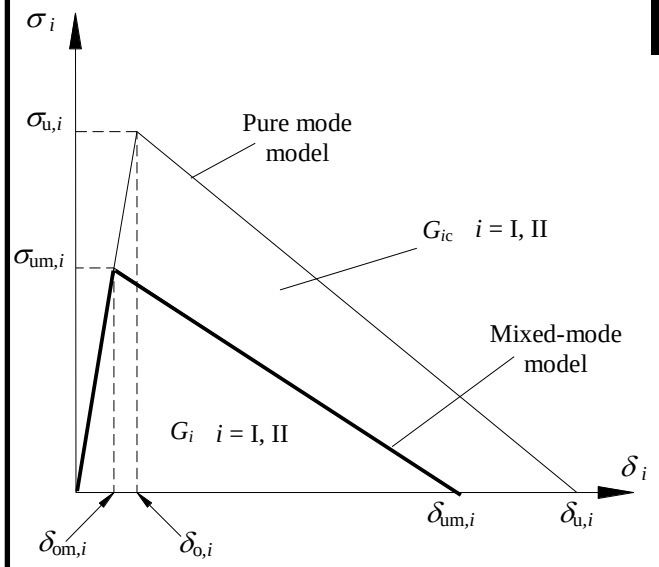

Figure 18. The linear softening law for pure and mixed-mode cohesive damage model.

b quadratic stress criterion to simulate damage initiation

$$\left(\frac{\sigma_{\mathrm{I}}}{\sigma_{\mathrm{u,I}}}\right)^2+\left(\frac{\sigma_{\mathrm{II}}}{\sigma_{\mathrm{u,II}}}\right)^2=1 \qquad (15)$$

c the linear energetic criterion to deal with damage growth

$$\left(\frac{G_{\mathrm{I}}}{G_{\mathrm{Ic}}}\right)+\left(\frac{G_{\mathrm{II}}}{G_{\mathrm{IIc}}}\right)=1 \qquad (16)$$

non-conventional tests [mixed-mode I+II]

It is useful to define the displacement ratio

$\lambda = \delta_L / \delta_R$

- $\lambda = -1$ pure mode I
- $\lambda = 1$ pure mode II

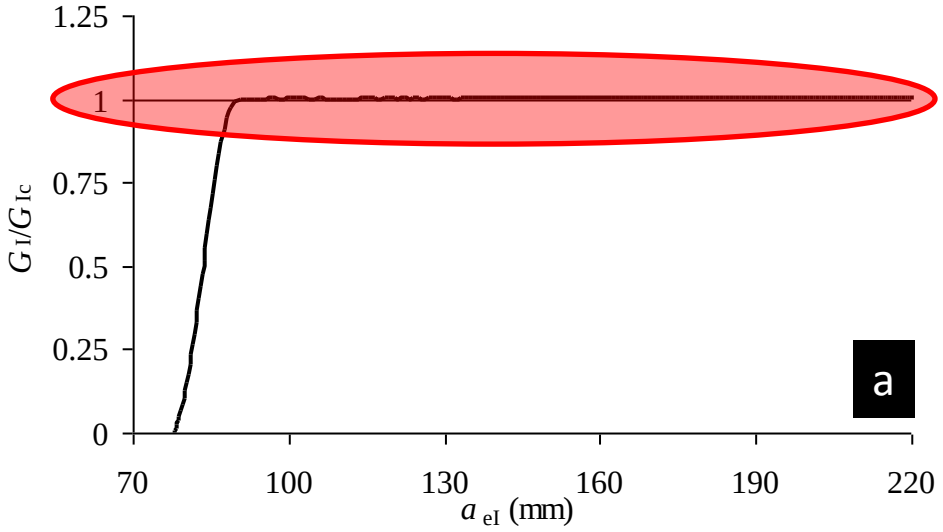

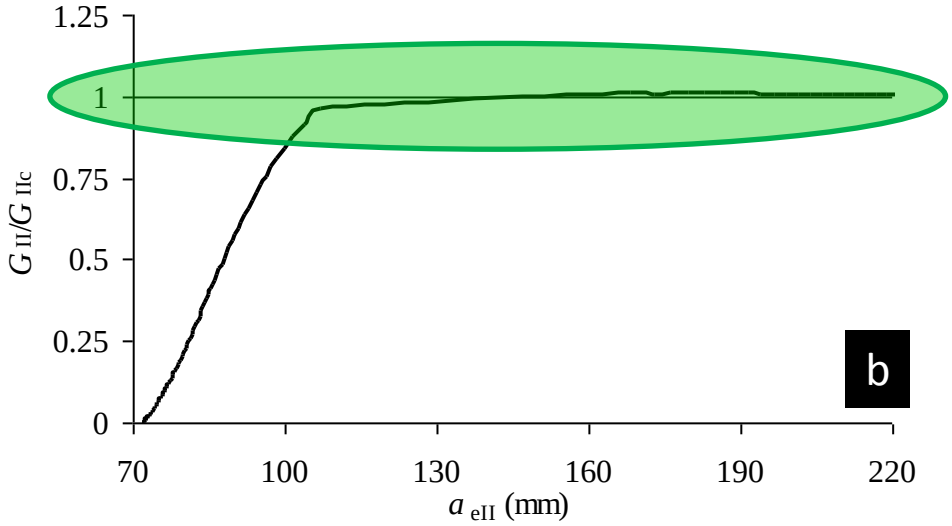

Figure 19. Normalized *R*-curves for the pure modes loading: a) Mode I; b) Mode II.

non-conventional tests [mixed-mode I+II]

six different cases were considered in the range $-0.9 \leq \lambda \leq -0.1$

in this case mode I loading clearly predominates

nine combinations were analysed for $0.1 \leq \lambda \leq 0.9$

a large range of mode ratios is covered

Table 5. Imposed displacements for each simulation

	imposed displacem.	
Simul. #	beam 1	beam 2
1	10	-9
2	10	-8
3	10	-7
4	10	-5
5	10	-3
6	10	-1
7	10	0
8	10	1
9	10	3
10	10	5
11	10	7
12	10	7.5
13	10	8
14	10	8.5
15	10	9

non-conventional tests [mixed-mode I+II]

variation of mode-mixity as the crack grows

for $\lambda = 0.7$, the *R*-curves vary as a function of crack length

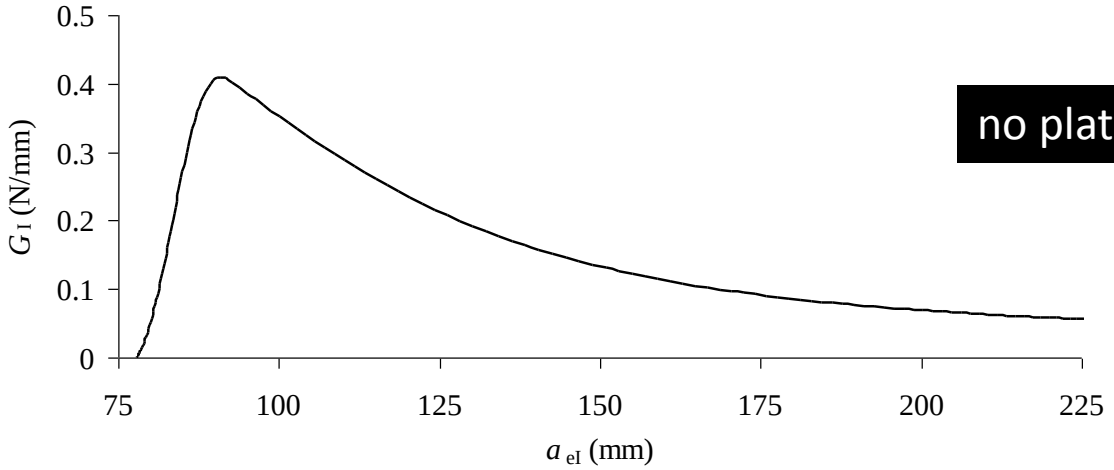

no plateau

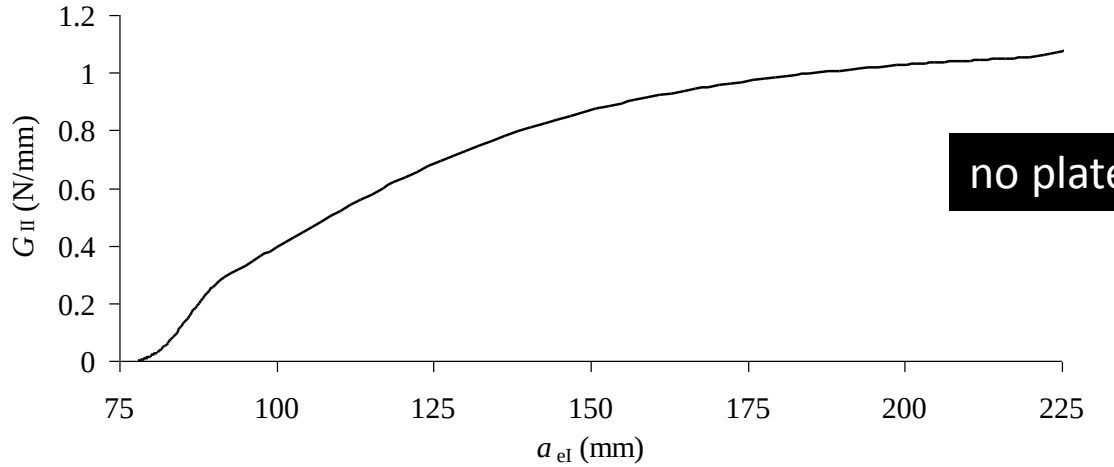

no plateau

Figure 20. *R*-curves for $\lambda = 0.7$ (both curves were plotted as function of a_{el} for better comparison).

non-conventional tests [mixed-mode I+II]

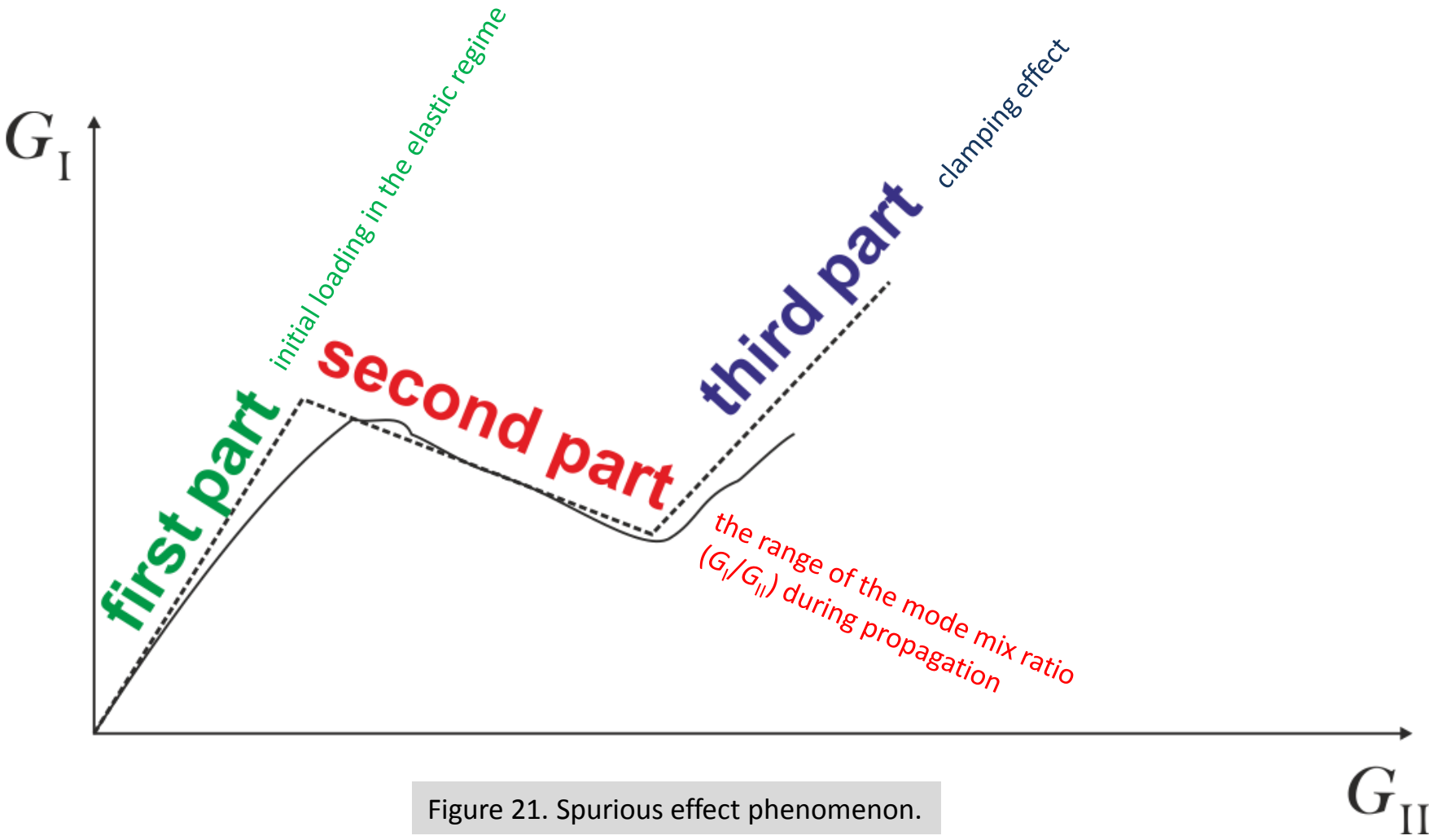

Figure 21. Spurious effect phenomenon.

the curves were cut at the beginning of the inflexion caused by the referred effects

- non-conventional tests [mixed-mode I+II]

mode I predominant loading conditions

combinations -0.9 ≤ λ ≤ -0.7, are nearly pure mode I loading conditions

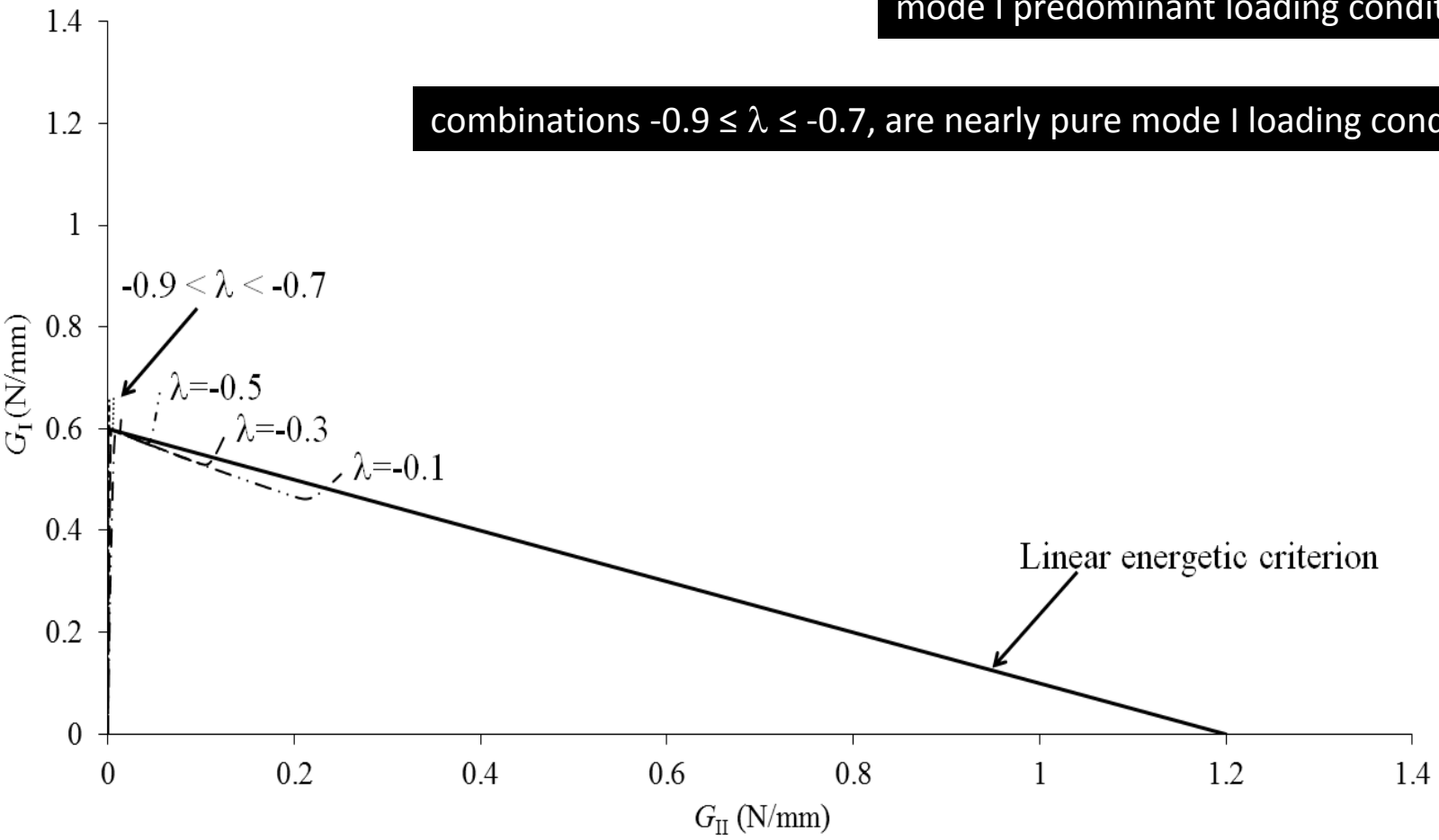

Figure 22. Plot of the G_I versus G_{II} strain energy components for -0.9 ≤ λ ≤ -0.1.

non-conventional tests [mixed-mode I+II]

combinations using the positive values of λ induce quite a large range of mode ratios during crack propagation

excellent reproduction of the inputted linear criterion in the vicinity of pure modes, presenting a slight difference where mixed-mode loading prevail

explained by the non self-similar crack growth, which is more pronounced in these cases

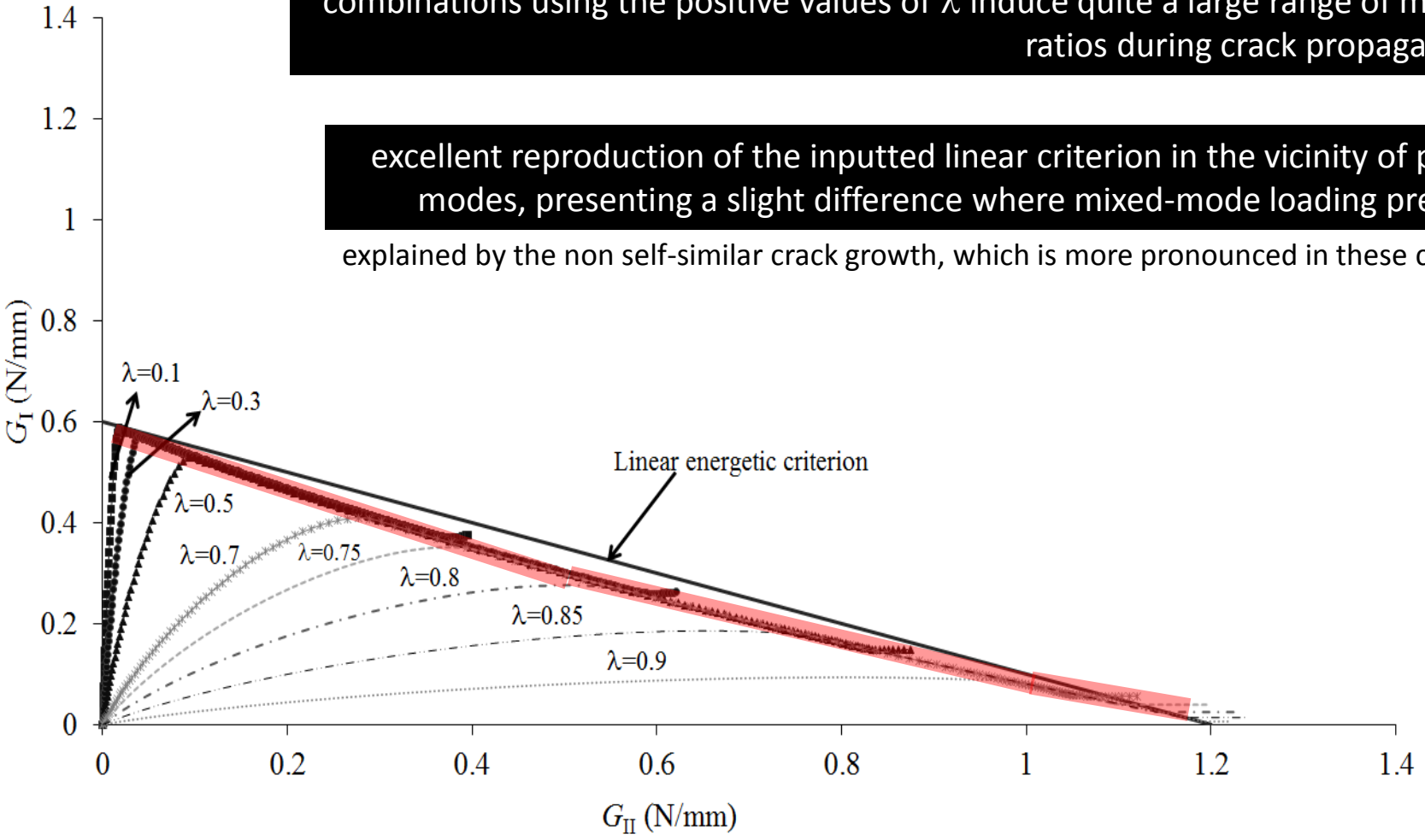

Figure 23. Plot of the G_I versus G_{II} strain energies for $0.1 \leq \lambda \leq 0.9$.

non-conventional tests [mixed-mode I+II]

practically the entire fracture envelope can be obtained using only two combinations ($\lambda = 0.1$ and $\lambda = 0.75$) **important advantage of the DAL test**

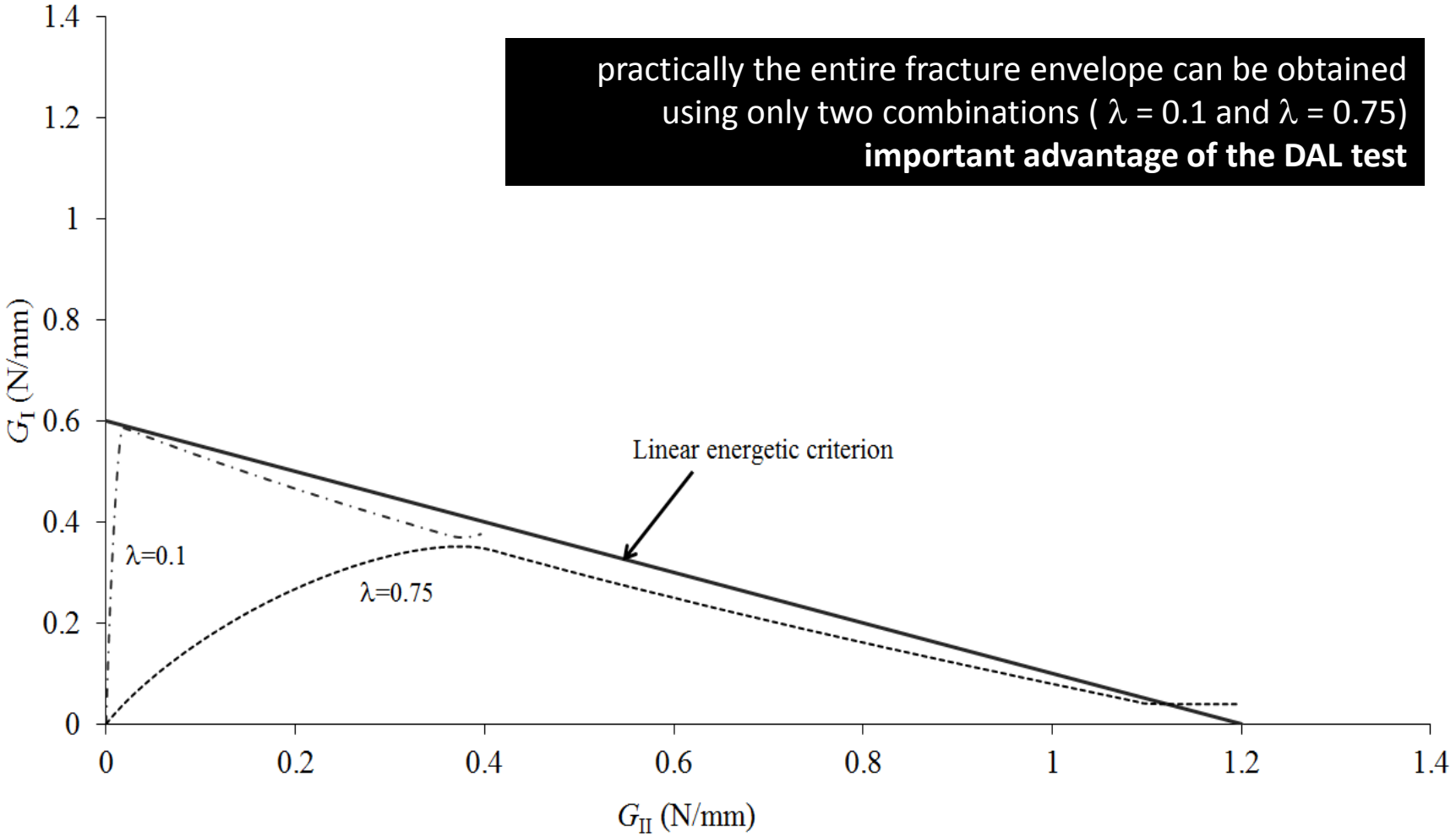

Figure 24. Plot of the G_I versus G_{II} strain energies for $\lambda = 0.1$ and $\lambda = 0.75$.

- non-conventional tests [mixed-mode I+II]

From table 3.

$$\begin{cases} G_I = 0.44 \pm 0.05 \text{ [N/mm]} \\ G_{II} = 2.1 \pm 0.21 \text{ [N/mm]} \end{cases}$$

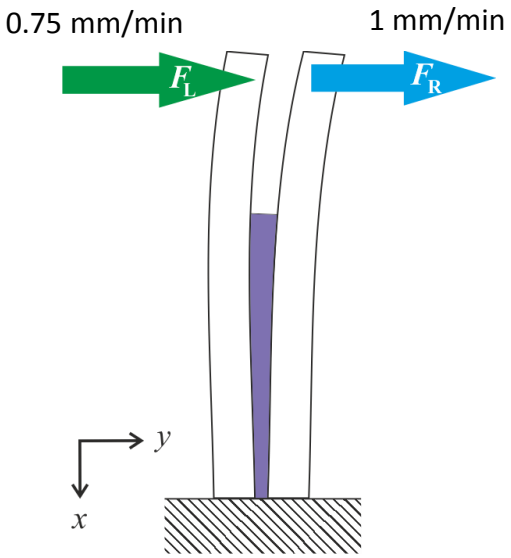

Figure 25. Schematic representation of loading scheme 2 with $\lambda = 0.75$.

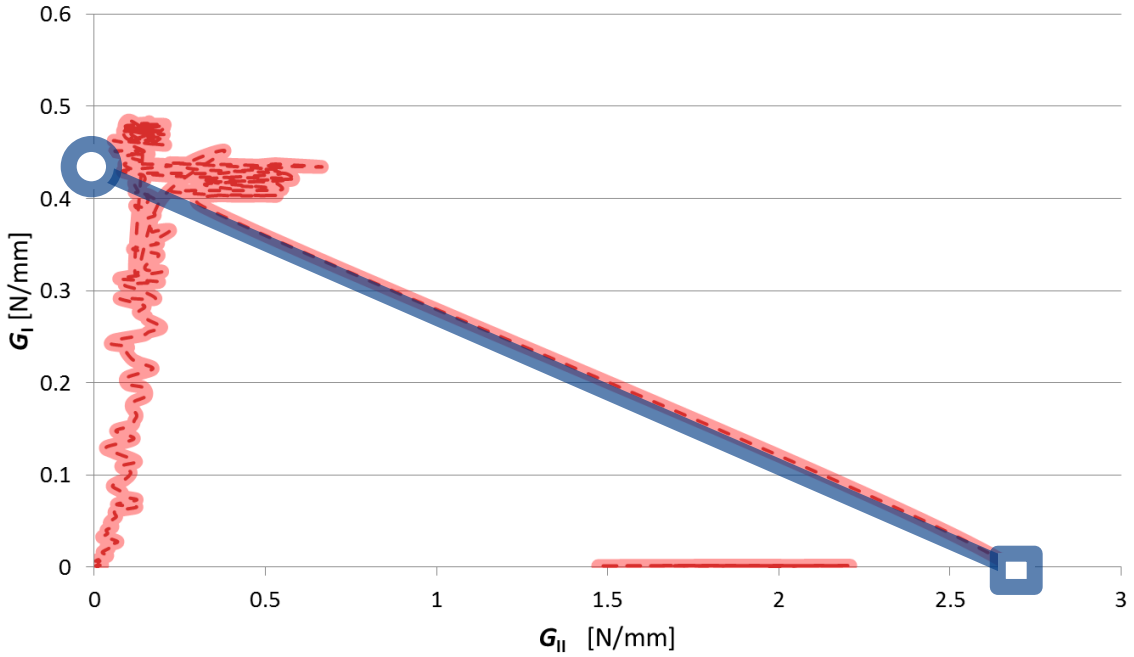

Figure 26. Envelope for Araldite 2015 with 0.2 mm bondline and $\lambda = 0.75$.

non-conventional tests [mixed-mode I+II]

Mixed-mode testing is being implemented with a specimen load jig similar to the one that Spelt proposed, using DCB specimens used for the pure mode I (DCB) and pure mode II (ENF) and also for mixed-mode DAL.

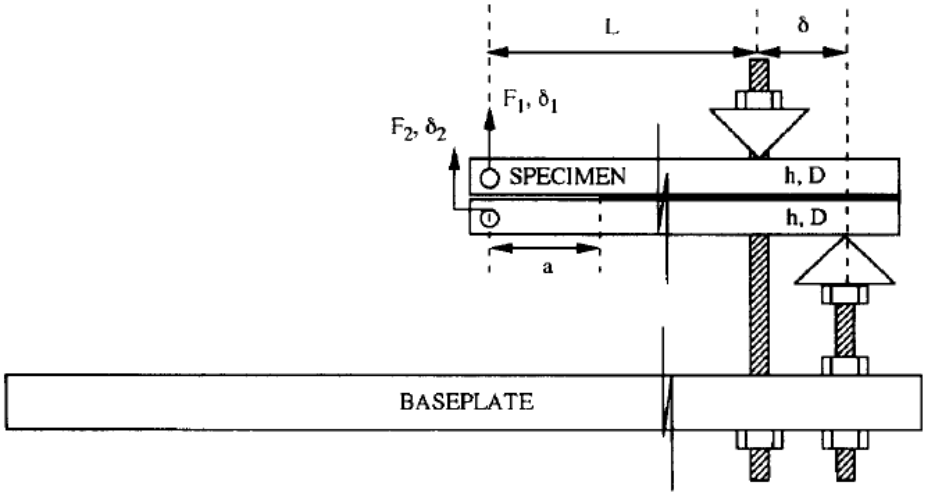

G. Fernlund & J. K. Spelt, *Composites Science and Technology* **50** (1994) 441-449

Figure 27. Load jig specimen geometry.

Figure 28. Specimen tested with the Spelt load jig.

non-conventional tests [mixed-mode I+II]

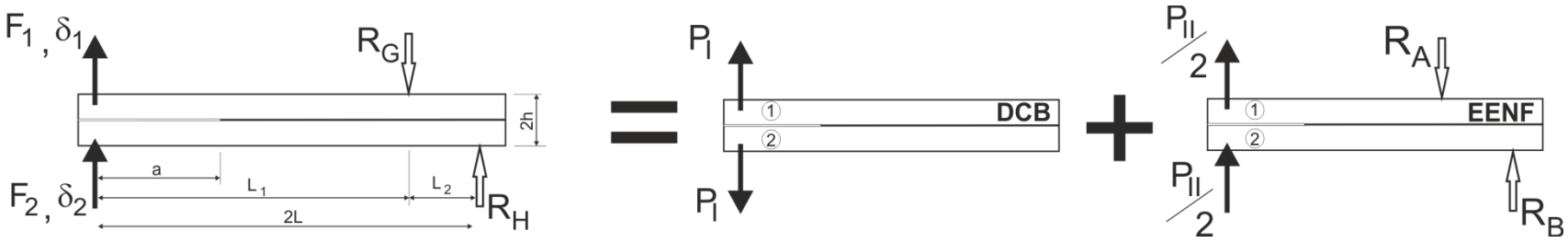

Figure 29. Schematic representation of loading in the SPELT test.

pure mode loading

$$P_I = \frac{F_1 - F_2}{2} \qquad P_{II} = F_1 + F_2 \tag{17}$$

pure mode displacements

$$\delta_I = \delta_1 - \delta_2 \qquad \delta_I = \frac{\delta_1 + \delta_2}{2} \tag{18}$$

(19) $R_G = \frac{(F_1+F_2)2\,L}{2L-L_1}$ and $R_H = \frac{(F_1+F_2)\,L_1}{2L-L_1}$

$$R_A = \frac{2\,L\,P_{II}}{2L - L_1} \quad and \quad R_B = \frac{P_{II}L_I}{2L - L_1} \tag{20}$$

- non-conventional tests [mixed-mode I+II]

Assuming $G = \frac{E}{2(1+\upsilon)}$, the pure compliances become:

(21) $$C_I = \frac{8a^3}{Ebh^3} + \frac{24 \cdot a(1+\upsilon)}{5Ebh}$$

(22) $$C_{II} = \frac{1}{E\,I}\left(a^3 + \frac{2}{3}\,L\,L_1^2\right) + \frac{12\,L_1\,L\,(1+\upsilon)}{5\,E\,b\,h\,(2L-L_1)}$$

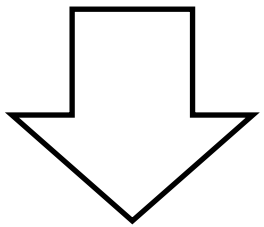

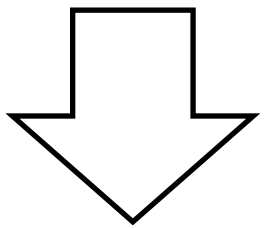

(23) $$G_I = \frac{12\,P_I^2}{E_{f,I}b^2h}\left(\frac{a_{e,I}^2}{h^2} + \frac{1+\upsilon}{5}\right)$$

(24) $$G_{II} = \frac{3\,P_{II}^2\,a_{e,II}^2}{2\,E_{f,II}\cdot I}$$

- non-conventional tests [mixed-mode I+II]

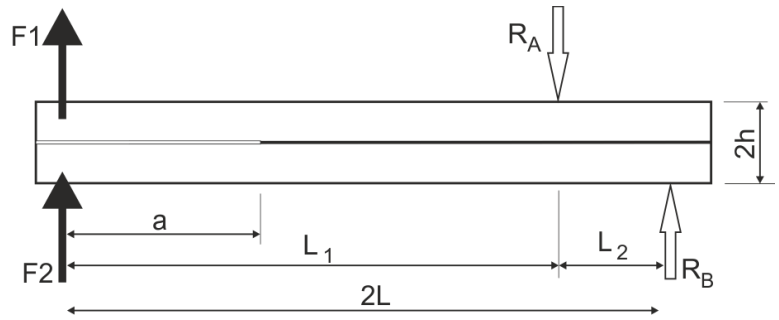

h = 12.7 mm

2L = 260 mm

L_2 = 35 mm

b = 25 mm

Figure 30. Specimen geometry used in the simulations of the SPELT test

Numerical analysis including a cohesive damage model was carried out to verify the performance of the test and the adequacy of the proposed data reduction scheme.

Table 4. Elastic and cohesive properties.

Elastic properties (Steel)		Cohesive properties (Adhesive)			
E (GPa)	G (MPa)	$s_{u,I}$ (MPa)	$s_{u,II}$ (MPa)	G_{Ic} (N/mm)	**G_{IIc} (N/mm)**
210	**80.77**	**23**	**23**	**0.6**	**1.2**

The specimen was modelled with 3992 plane strain 8-node quadrilateral elements and 382 6-node interface elements with null thickness placed at the mid-plane of the bonded specimen.

non-conventional tests [mixed-mode I+II]

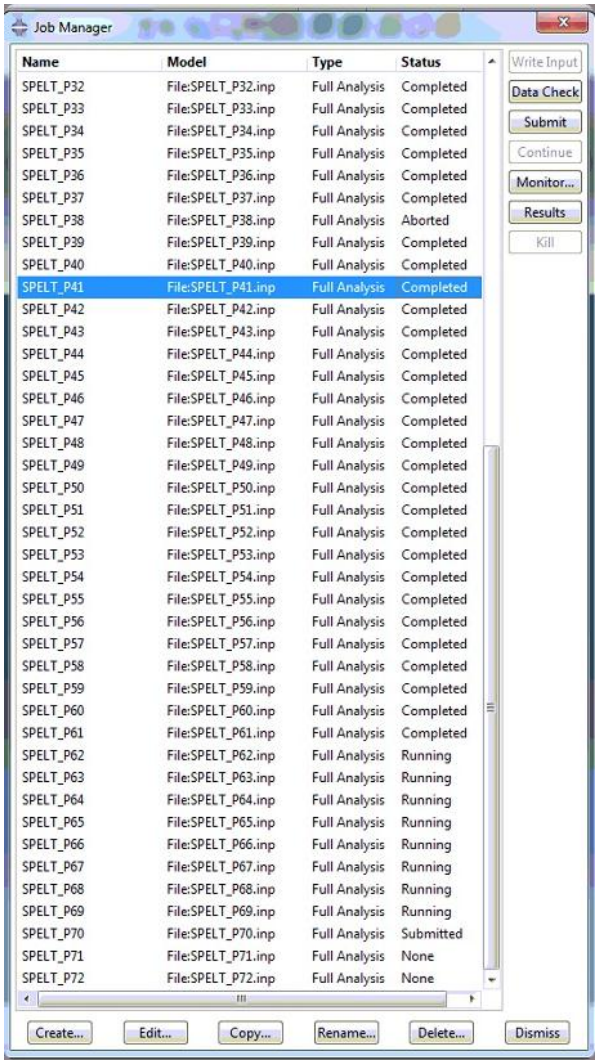

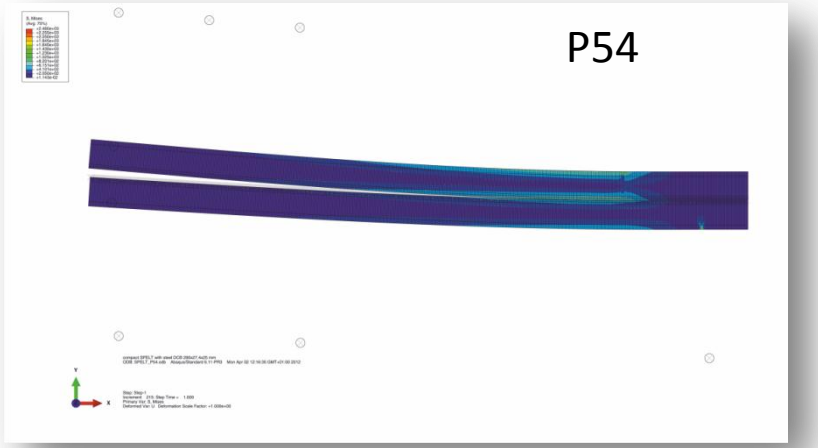

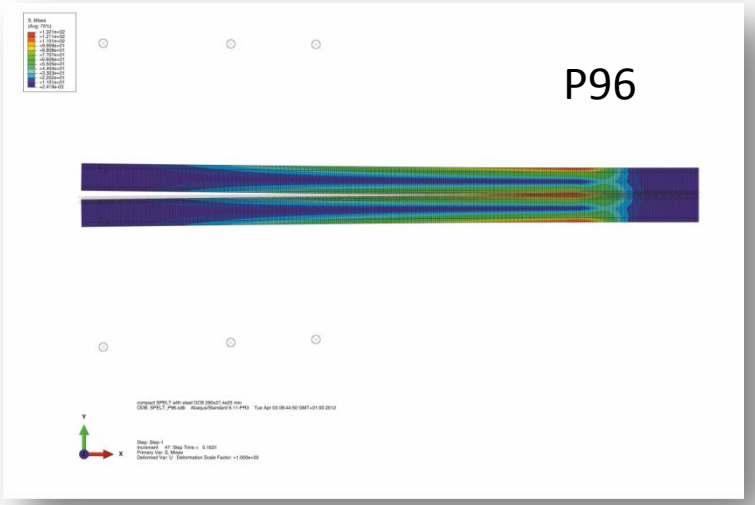

Figure 31. Job manager (left) and two combinatons .

non-conventional tests [mixed-mode I+II]

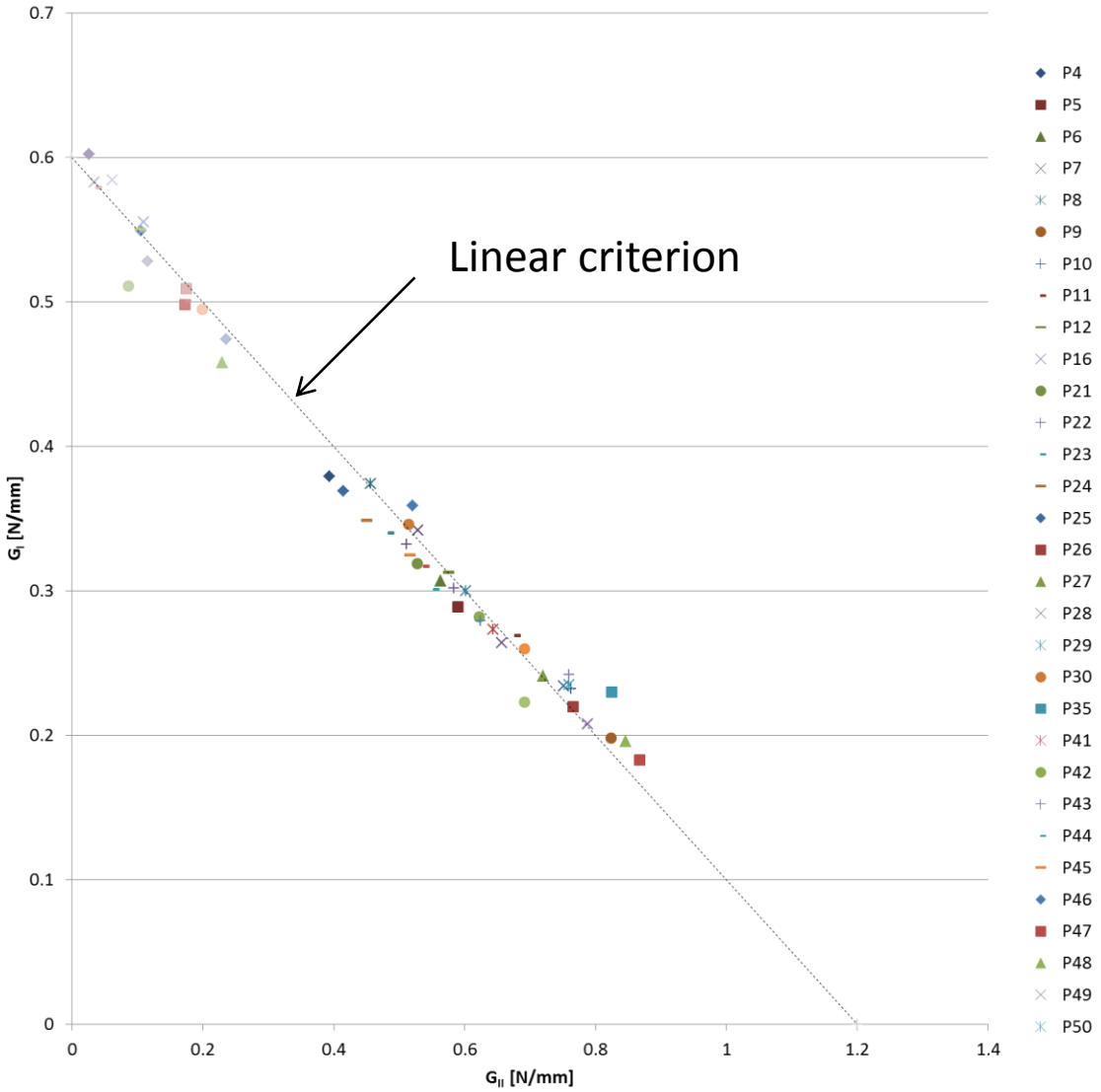

Figure 32. Spelt numerical fracture envelope plot.

non-conventional tests [mixed-mode I+II]

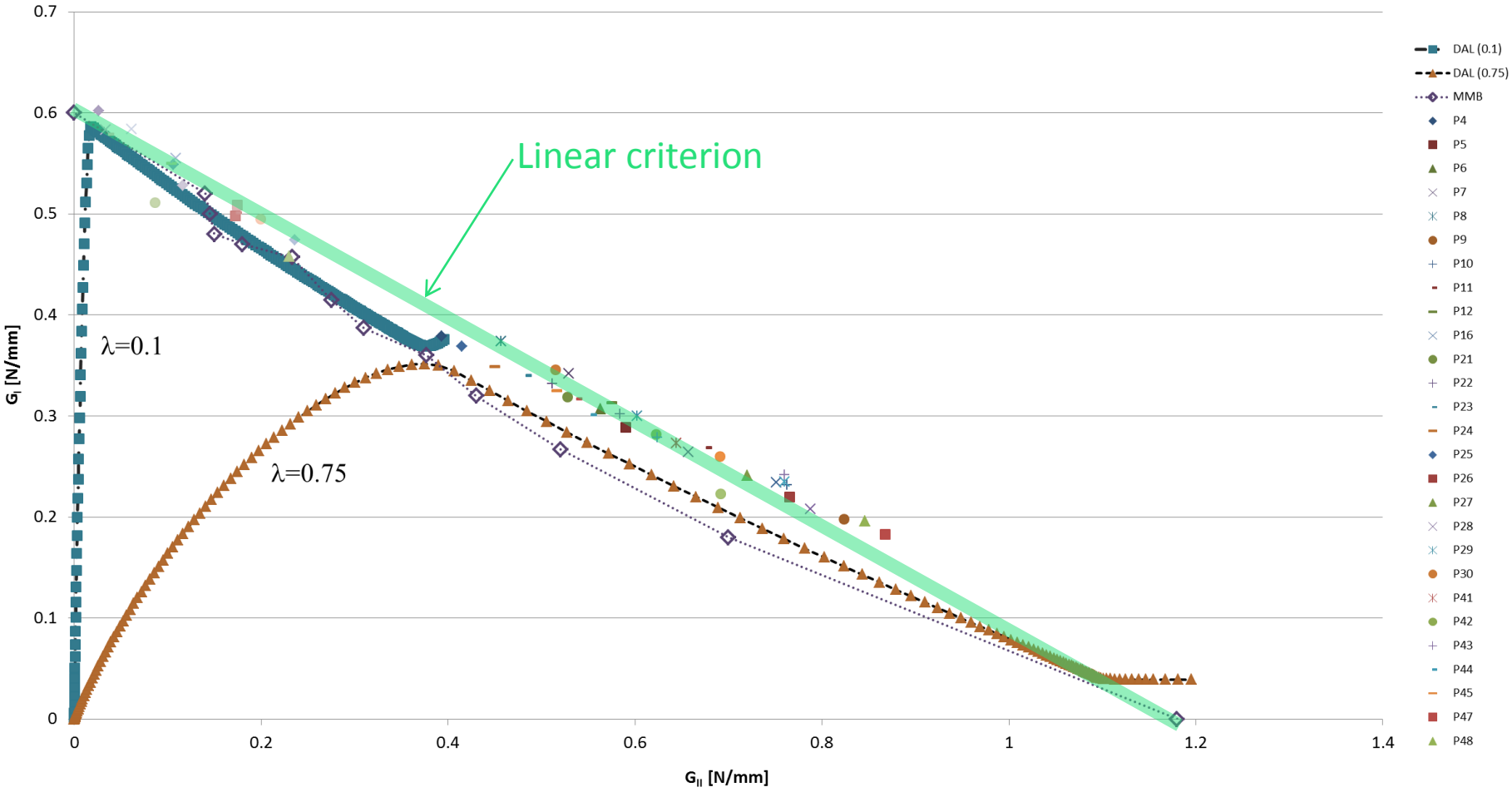

Figure 33. numerical envelope plot for MMB, DAL and SPELT.

non-conventional tests [mixed-mode I+II]

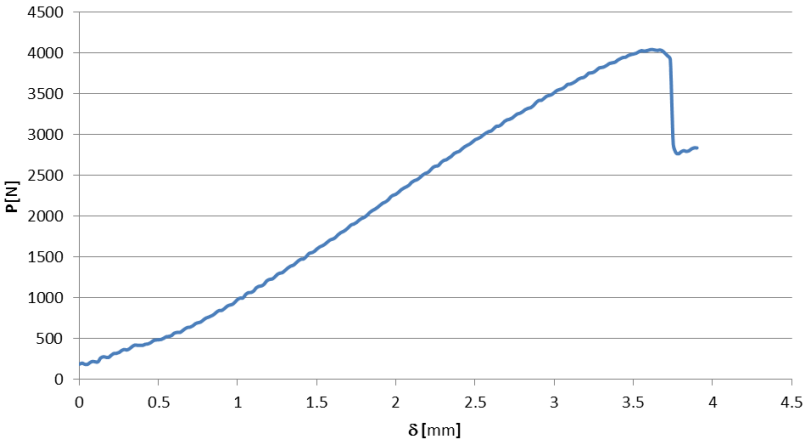

Figure 34. P-δ curve for $\Psi = 56^o$

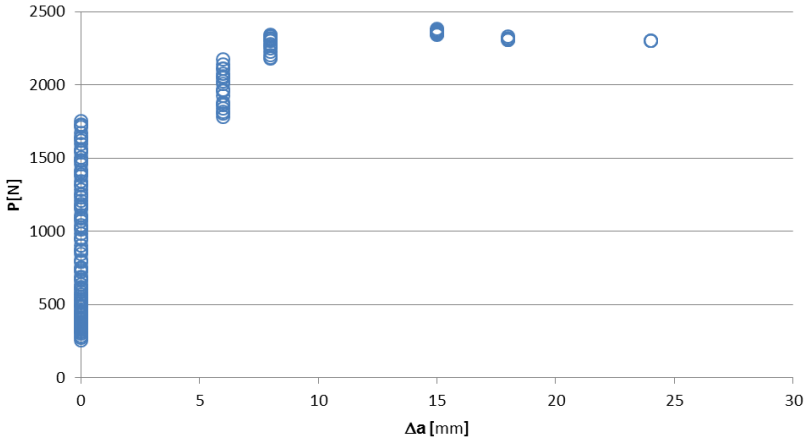

Figure35. P-Δa curve for $\Psi = 56^o$

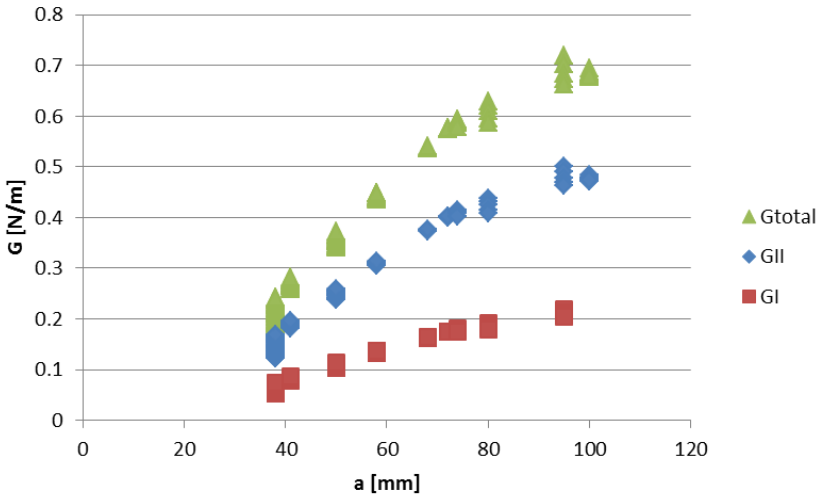

Figure 36. R curve for $\Psi = 56^o$

- non-conventional tests [mixed-mode I+II]

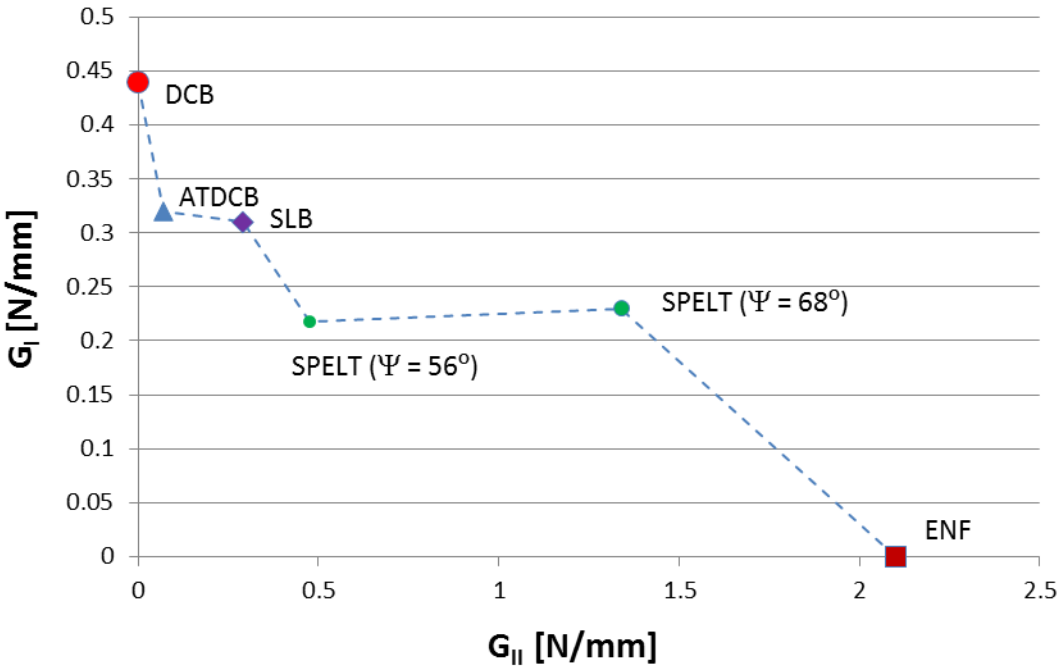

Figure 37. Experimental envelope (Araldite 2015)

non-conventional tests [mixed-mode I+II]

- a new data reduction scheme based on specimen compliance, beam theory and crack equivalent concept was proposed to overcome some problems intrinsic to the DAL and SPELT tests
- the model provides a simple mode partitioning method and does not require crack length monitoring during the test, which can lead to incorrect estimation of fracture energy due to measurements errors
- since the current compliance is used to estimate the equivalent crack length, the method is able to account indirectly for the presence of a non-negligible fracture process zone (very important for ductile adhesives)
- for pure modes I and II, excellent agreement was achieved with the fracture values inputted in the cohesive model
- for DAL tests a slight difference relative to the inputted linear energetic criterion was observed in the central region of the G_I versus G_{II} plot, corresponding to mixed-mode loading, which is attributed to the non self-similar crack propagation conditions that are more pronounced in these cases. The SPELT test has a nearly constant mixed-mode, providing better results for this central region of the fracture envelope.
- with the DAL test only two combinations of the displacement ratio are sufficient to cover almost all the fracture envelope

conclusions

The authors would like to thank the contribution of Edoardo Nicoli, and Youliang Guan for their work in experimental testing at Virginia Tech.

The authors also acknowledge the financial support of Fundação Luso Americana para o Desenvolvimento (FLAD) through project 314/06, 2007 , IDMEC and FEUP.

Thank you.

conventional – using the crack length measurement [a}

Compliance Calibration Method (CCM) is based on the Irwin-Kies theory (Trantina 1972, Kanninen and Popelar 1985)

Direct Beam Theory (DBT), based on elementary beam theory (Ding 1999)

Corrected Beam Theory (CBT) (Robinson and Das 2004, Wang and Williams 1992)

non-conventional – using the equivalent crack length [a_e]

The Compliance Based Beam Method (CBBM) was recently developed by de Moura et al. (2008, 2009) and is based on the crack equivalent concept